Energy 39 (2012) 236–245

Contents lists available at SciVerse ScienceDirect

Energy

journal homepage: www.elsevier.com/locate/energy

# Design of heat sink for improving the performance of thermoelectric generator using two-stage optimization

Chien-Chang Wang [a], Chen-I Hung [a,**], Wei-Hsin Chen [b,*]

[a] Department of Mechanical Engineering, National Cheng Kung University, Tainan 701, Taiwan, ROC
[b] Department of Greenergy, National University of Tainan, Tainan 700, Taiwan, ROC

ARTICLE INFO

*Article history:*
Received 16 October 2011
Received in revised form
6 January 2012
Accepted 13 January 2012
Available online 16 February 2012

*Keywords:*
Thermoelectric generator (TEG)
Heat sink design
Two-stage optimization
Compromise programming
Scaling effect
Finite element scheme

ABSTRACT

Thermoelectric (TE) devices can provide clean energy conversion and are environmentally friendly; however, little research has been published on the optimal design of air-cooling systems for thermoelectric generators (TEGs). The present study investigates the performance of a TEG combined with an air-cooling system designed using two-stage optimization. An analytical method is used to model the heat transfer of the heat sink and a numerical method with a finite element scheme is employed to predict the performance of the TEG. In the first-stage optimization, the optimal fin spacing for a given heat sink geometry is obtained in accordance with the analytical method. In the second-stage optimization, called compromise programming, decreasing the length of the heat sink by increasing its frontal area ($W_{HS}H_f$) is the recommended design approach. Using the obtained compromise point, though the heat sink efficiency is reduced by 20.93% compared to that without the optimal design, the TEG output power density is increased by 88.70%. It is thus recommended for the design of the heat sink. Moreover, the TEG power density can be further improved by scaling-down the TEG when the heat sink length is below 14.5 mm.



## 1. Introduction

Over the last several decades, there has been a dramatic progress in the development of green energy technology which can reduce greenhouse gas emissions and fossil fuel usage. Thermoelectric (TE) devices, which consist of p-type and n-type semiconductors, can be considered as a useful tool to practice the green energy technology. TE devices can be divided into two types, namely thermoelectric coolers (TECs) [1–4] and thermoelectric generators (TEGs) [5–8]. TECs convert electricity into thermal energy for cooling via the Peltier effect, whereas, TEGs convert thermal energy, say, waste heat, into electrical power via the Seebeck effect.

Unlike convectional heat engines or compression refrigerators, TE devices are solid-state; they contain neither moving parts nor refrigerants [9]. Therefore, the whole system can be simplified and operated over an extended period of time without maintenance [10]. TE devices can produce energy without using fossil fuel and can thus reduce greenhouse gas emissions. However, the energy conversion efficiency of TE devices is lower than those of convectional heat engines or refrigerators [11]. The efficiency of TEGs and the coefficient of performance (COP) of TECs are functions of not only the figure of merit (ZT) but also the temperature difference across the devices [12]. ZT is the performance index of a thermoelectric material. Its value is relatively low (about 1.0) for the best existing commercial TE cooling modules whereas that for conventional air-conditioning system is about 4.0 [13]. Consequently, a strategy for improving the performance of TE devices is needed.

In reviewing past research concerning thermal design of TEGs, a number of studies have been reported. For example, Esarte et al. [14] employed a theoretical method to analyze the influence of the design parameters of heat exchangers on the power supplied by a TEG. The theoretical results well matched the experimental values for low flow rates but not for high flow rates. Chen et al. [15] found that heat transfer irreversibility affected the performance of TEG and thus had to be considered in analysis. A TEG system combined with the heat exchangers at both the hot and cold side was numerically modeled by Astrain et al. [16]. Their results showed that when the thermal resistances of heat exchangers on both sides of the TEG were decreased by 10%, the TEG output power was increased by 8%.

Recently, waste heat has been recovered for further usage. Waste heat can be used for space and water heating [17,18],

* Corresponding author. Tel.: +886 6 2605031; fax: +886 6 2602205.
** Corresponding author. Tel.: +886 6 2757575x62169; fax: +886 6 2352973.
*E-mail addresses:* cihung@mail.ncku.edu.tw (C.-I. Hung), weihsinchen@gmail.com (W.-H. Chen).

0360-5442/$ – see front matter 
doi:10.1016/j.energy.2012.01.025

**Nomenclature**

| | |
|---|---|
| $A_c$ | Cross-sectional area (mm$^2$) |
| $A$ | Surface area (mm$^2$) |
| $C_p$ | Specific heat at constant pressure (kJ kg$^{-1}$ K$^{-1}$) |
| $D_{TE}$ | Depth of TE element (mm) |
| $D_g$ | Fin-to-fin spacing (mm) |
| $\vec{E}$ | Electric field intensity vector (V m$^{-1}$) |
| $f$ | Distance function in the compromise programming |
| $G$ | Ratio of the cross-sectional area to length of TE element (mm) |
| $H_f$ | Fin height (mm) |
| $\bar{h}$ | Average heat transfer coefficient of the fins (W m$^{-2}$ K$^{-1}$) |
| $h$ | Heat transfer coefficient (W m$^{-2}$ K$^{-1}$) |
| $I$ | Electric current (A) |
| $\vec{J}$ | Electric current density vector (A m$^{-2}$) |
| $k$ | Thermal conductivity (W m$^{-1}$ K$^{-1}$) |
| $L$ | Length (mm) |
| $N_f$ | Number of fins |
| $N_{TE}$ | Number of TEG couple |
| $P$ | Output power of TEG (mW) |
| $P''$ | Output power density of TEG, $\equiv P/A_{c,TE}$ (mW mm$^{-2}$) |
| $P_f$ | Fin perimeter (mm) |
| $\Delta p$ | Pressure drop across the heat sink (N m$^{-2}$) |
| $Pr$ | Prandtl number, $\equiv \nu/\alpha$ |
| $\dot{q}$ | Heat generation per unit volume (W m$^{-3}$) |
| $\vec{q}$ | Heat flux vector (W m$^{-2}$) |
| $Q$ | Heat transfer rate (W) |
| $Q_l$ | Heat transfer rate for the boundary layer flow limit (W) |
| $Q_s$ | Heat transfer rate for the fully developed flow limit (W) |
| $R$ | Electric resistance ($\Omega$) |
| $S$ | Seebeck coefficient (V K$^{-1}$) |
| $T$ | Absolute temperature (K) |
| $T_w$ | Surface temperature of the fins (K) |
| $T_\infty$ | Fluid inlet temperature (K) |
| $t_f$ | Fin thickness (mm) |
| $V$ | Total volume of heat sink (mm$^3$) |
| $W$ | Width (mm) |
| $X$ | Geometry parameter of the heat sink (mm) |
| $(x,y)$ | Real point in the compromise programming |
| $(x^*,y^*)$ | Ideal point in the compromise programming |
| $ZT$ | Dimensionless TE figure of merit |

*Greek letters*

| | |
|---|---|
| $\alpha$ | Fluid thermal diffusivity (m$^2$ s$^{-1}$) |
| $\varphi$ | Electric scalar potential (V) |
| $\eta$ | Efficiency (%) |
| $\mu$ | Fluid viscosity (N s m$^{-2}$) |
| $\nu$ | Fluid kinematic viscosity (m$^2$ s$^{-1}$) |
| $\rho$ | Fluid density (kg m$^{-3}$) |
| $\rho_e$ | Electrical resistivity ($\Omega$ m) |

*Subscripts*

| | |
|---|---|
| $B$ | Heat sink base |
| base | Base case |
| $c$ | Cold side of TE element |
| eff | Effective |
| $F$ | Fluid |
| $f$ | Fin |
| HS | Heat sink |
| $h$ | Hot side of TE element |
| $L$ | External load |
| loss | Heat loss from the side surfaces of the TE element |
| max | Maximum |
| $n$ | n-type for TE element |
| opt | Optimum |
| $p$ | p-type for TE element |
| TE | Thermoelectric element |
| $t$ | Total heat sink heat transfer area |

improving energy recovery efficiency and system efficiency [19,20], and enhancing chemical reactions [21,22]. Moreover, several studies [23,24] have shown the promising potential of using TEGs for waste heat recovery. Meng et al. [25] proposed a TEG model with multi-irreversibilities; they suggested that the results could be regarded as the feasibility reference using the waste heat for power generation. Because there is almost no cost for obtaining waste heat, the low efficiency problem of TE devices is not a critical issue [24].

Some studies have optimized the geometric design of TE devices. A numerical optimization of a TEC was presented by Xuan [26]. The results indicated that the construction cost of a TEC was closely related to the cooling power density, whereas the running cost was inversely proportional to COP. Kubo et al. [27] altered the size of incisions along the lateral faces of a TE device; they found that the relationship between the TE performance and the incision size depended on the cold side temperature. Yilbas and Sahin [28] introduced two parameters, the slenderness ratio and the external load parameter, to analyze the TEG efficiency; their results showed that the higher efficiency could be obtained for almost all the external load parameters considered when the slenderness ratio was less than 1. Jang et al. [29] optimized the design of micro-TEGs using finite element analysis. High efficiency was obtained when the length of the thermoelements was large. In addition, the power generated declined with the cross-sectional area of the thermoelements, whereas efficiency showed the opposite trend.

A review of the literature shows that the design of the geometry plays an important role in optimizing the performance of TEGs. However, few studies have reported on the optimization of geometry design of TEGs incorporated with air-cooling system. An air-cooling system combined with a heat sink is commonly used for dissipating the heat produced by electronic devices due to its low unit price, low weight, and high reliability [30]. Accordingly, the objective of the present study is to investigate the characteristics of TEGs with an air-cooling design where a finite element method is used to predict the performance of the TEGs. The effects of the heat sink geometry and TEG dimensions on performance are taken into account. To improve the performance of the TEGs, two-stage optimization is carried out. Specifically, an analytical method is used to model the air-cooling system, followed by employing a method of compromise programming to seek the optimal performance of TEGs.

## 2. Mathematical formulation and modeling

Numerical simulations are adopted to predict the performance of TEGs. The physical and numerical models are described below.

### 2.1. Assumptions

To simplify the TEG system, the following assumptions are made:

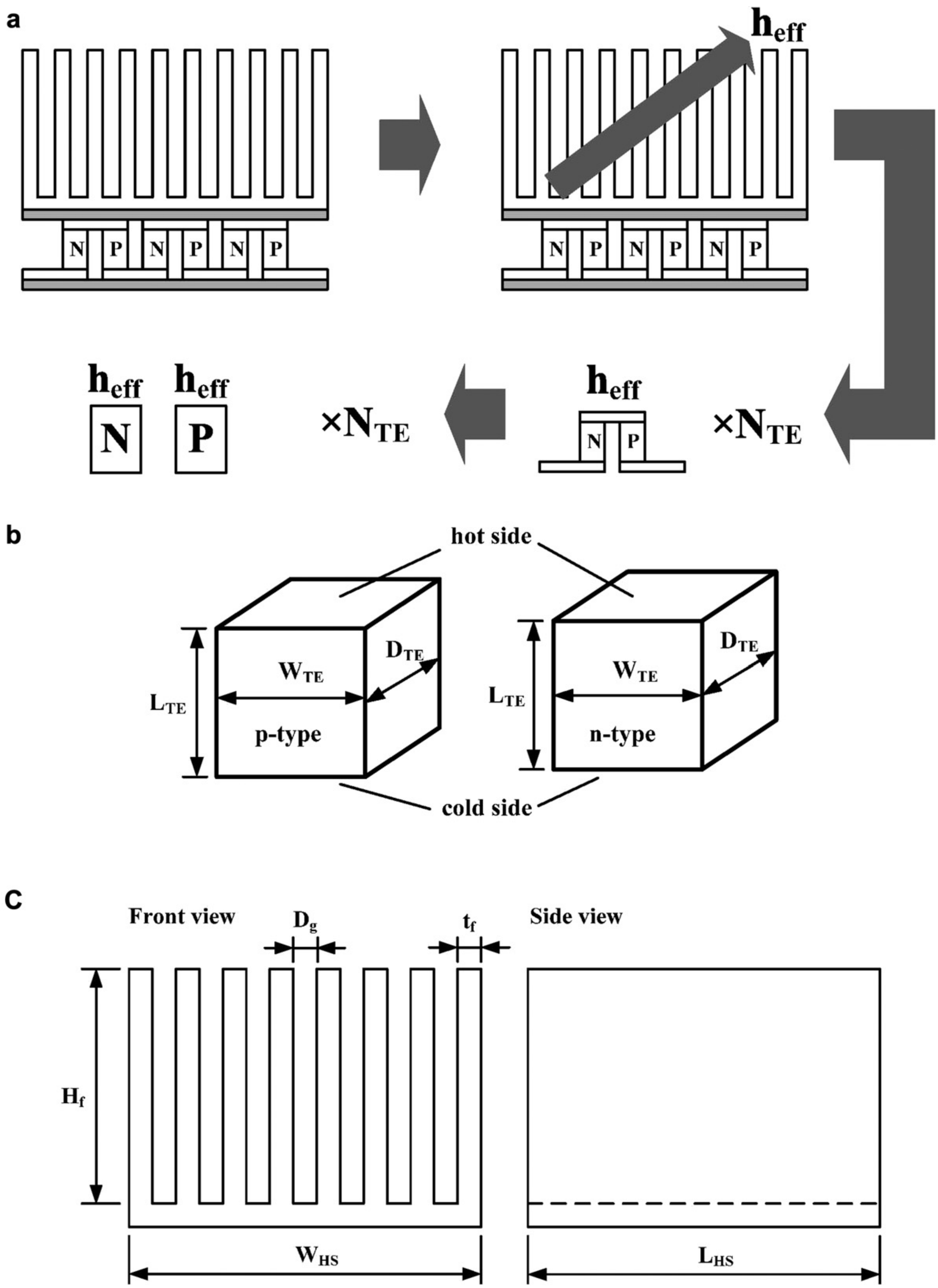


**Fig. 1.** Schematics of (a) simplified system, (b) thermoelectric couple geometry, and (c) heat sink geometry.

(1) the system is steady-state;
(2) the existence of electrodes is ignored and the contact resistances are neglected because the length of the thermoelectric element is larger than 200 μm [31];
(3) the material properties of the thermoelectric elements are independent of temperature;
(4) the configurations of the p-type and n-type elements are equivalent;

(5) the TEG module is constructed from thermoelectric couples which are identical and joined in series;
(6) the heat sink is not included in the computational domain but transformed into a boundary condition using the analytical method; and
(7) the airflow around the heat sink is assumed to be laminar because of small fin space and low flow rate typically encountered in electrical device cooling [32].

Based on the above assumptions, the simplification of the TEG module is illustrated in Fig. 1a. One thermoelectric couple comprising a p-type and an n-type elements is simulated in this study. In Fig. 1b, the geometry of the thermoelectric element is specified by the element depth $D_{TE}$, element width $W_{TE}$, and element length $L_{TE}$. In the simulation, the p-type and n-type elements are connected electrically in series and thermally in parallel.

### 2.2. Governing equations for TEG

In order to analyze the thermoelectric system, the governing equations include the thermal, electrical, and thermoelectric effects. Therefore, the conservation principles of energy and current are considered simultaneously [29]:

$$\nabla \cdot \vec{q} = \dot{q} \tag{1}$$

$$\nabla \cdot \vec{J} = 0 \tag{2}$$

where $\vec{q}$, $\vec{J}$, and $\dot{q}$ represent the heat flux vector, current density vector, and heat generation, respectively. The above equations can be coupled by the following constitutive equations:

$$\vec{q} = S_{TE} T \vec{J} - k_{TE} \nabla T \tag{3}$$

$$\vec{J} = \frac{1}{\rho_{e,TE}} (\vec{E} - S_{TE} \nabla T) \tag{4}$$

where $k_{TE}$, $S_{TE}$, and $\rho_{e,TE}$ are the thermal conductivity, Seebeck coefficient, and electrical resistivity of a thermoelectric element, respectively. Moreover, $\vec{E}$ is the electric field intensity vector which is derived from an electric scalar potential $\varphi$:

$$\vec{E} = -\nabla \varphi \tag{5}$$

By substituting Eqs. (3)–(5) into Eq. (1) and Eq. (2), the coupled governing equations for the electric potential and temperature are given by:

$$\nabla \cdot (S_{TE} T \vec{J}) - \nabla \cdot (k_{TE} \nabla T) = \dot{q} \tag{6}$$

$$\nabla \cdot \left( \frac{1}{\rho_{e,TE}} \nabla \varphi \right) + \nabla \cdot (S_{TE} \nabla T) = 0 \tag{7}$$

where the heat generation $\dot{q}$ in Eq. (6) generally includes the electric power $\vec{J} \cdot \vec{E}$ spent on Joule heating and on work against the Seebeck field $S_{TE} \nabla T$ [33].

### 2.3. Analytical modeling of heat sink

The heat sink geometry is shown in Fig. 1c. It is the most common configuration used in current applications [34]. In this figure, the heat sink comprises a series of parallel fins with height $H_f$, length $L_{HS}$, and thickness $t_f$. Each fin is spaced by a gap $D_g$ and mounted on the heat sink base with an area of $L_{HS} \times W_{HS}$. Air is employed as the coolant. The direction of the airflow is assumed to be parallel to the heat sink base. Due to the small fin spacing and low airflow rates, the airflow in typical plate fin heat sinks applied to electronic modules can be regarded as a laminar flow [32]. Therefore, the laminar-based analytical method proposed by Mereu et al. [35] is used to analyze and optimize the heat sink system [36].

In this method, the scale of the total heat transfer rate dissipated by the fins is divided into two extreme limits with one for narrow channels ($D_g/L_{HS} \to 0$) and the other for large channels ($D_g/L_{HS} \to \infty$) [34]. For the limit of narrow channels, the airflow is considered as a fully developed flow. The total heat transfer rate can thus be obtained using [35]:

$$Q_s = \frac{\rho W_{HS} H_f}{1 + t_f/D_g} \frac{D_g^2}{12\mu} \frac{\Delta p}{L_{HS}} C_p (T_w - T_\infty) \tag{8}$$

where $\rho$ is the fluid density, $\mu$ is the fluid viscosity, $C_p$ is the specific heat at constant pressure, $\Delta p$ is the pressure drop across the heat sink, $T_w$ is the maximum surface temperature of the fins, and $T_\infty$ is the fluid inlet temperature. It should be noted that the fin surfaces are assumed to be isothermal (i.e., $T_w$) for simplicity. For the limit of large channels, the fin-to-fin spacing is large enough so that the airflow is approximated as a boundary layer flow. Consequently, the total heat transfer rate is expressed as [35]:

$$Q_l = 1.208 k_F W_{HS} H_f \frac{T_w - T_\infty}{1 + t_f/D_g} \left( \frac{Pr L_{HS} \Delta p}{\rho \nu^2 D_g^2} \right)^{1/3} \tag{9}$$

where $k_F$ is the fluid thermal conductivity, $\nu$ is the fluid kinematic viscosity, and $Pr$ is the Prandtl number.

For a given heat sink volume $W_{HS} \times L_{HS} \times H_f$, there is an optimal fin-to-fin spacing $D_{g,opt}$ corresponding to the maximum heat transfer rate. The value of $D_{g,opt}$ can be obtained by intersecting the two asymptotes from Eq. (8) and Eq. (9), which yields:

$$\frac{D_{g,opt}}{L_{HS}} = 2.73 \left( \frac{\Delta p L_{HS}^2}{\mu \alpha} \right)^{-1/4} \tag{10}$$

Hence, the maximum heat transfer rate $Q_{max}$ corresponding to $D_{g,opt}$ can be obtained by substituting Eq. (10) into Eq. (8) or Eq. (9). Furthermore, in order to include the effect of the heat sink on the performance of the TEG, an effective heat transfer coefficient is used in this study [23,32]. The effective heat transfer coefficient is defined as:

$$h_{eff} = \frac{Q_{max}}{A_B (T_w - T_\infty)} \tag{11}$$

where $A_B$ is the base area of the heat sink. If the thermal resistance of the heat sink base is negligible, the influence of the heat sink geometry or fluid operating conditions can be characterized by the effective heat transfer coefficient, which can be imposed as a boundary condition in the simulation of the TEG.

### 2.4. Boundary conditions

The boundary conditions for the present simulation are as follows.

**Table 1**
Properties of thermoelectric elements [8].

| Material | Electric resistivity ($\Omega$m) | Thermal conductivity (W/mK) | Seebeck coefficient (V/K) |
|---|---|---|---|
| p-type | $1.447 \times 10^{-5}$ | 1.52 | $226.8 \times 10^{-6}$ |
| n-type | $1.447 \times 10^{-5}$ | 1.52 | $-226.8 \times 10^{-6}$ |

**Table 2**
Comparisons of numerical and analytical results ($T_h = 423$ K and $T_c = 303$ K).

| Quantity | Analytical results [8] | Grid system 1 (2432 grids) | Grid system 2 (4600 grids) | Grid system 3 (12,544 grids) |
|---|---|---|---|---|
| $Q_h$ (W) | 81.3 | 81.31 | 81.31 | 81.31 |
| $P$ (W) | 3.98 | 3.966 | 3.966 | 3.966 |
| $I$ (A) | 1.08 | 1.079 | 1.079 | 1.079 |
| $\eta_{TE}$ (%) | 4.89 | 4.878 | 4.878 | 4.878 |

(1) For the numerical validations, constant temperature $T_h$ and $T_c$ are applied at the hot side and cold side of the TEG elements, respectively. Furthermore, heat loss along the side surfaces of the TEG elements is taken into account by means of a uniform heat transfer coefficient $h_{loss}$.
(2) When the heat sink is considered, an effective heat transfer coefficient $h_{eff}$ instead of $T_c$ is employed at the cold side of the TEG elements. The heat loss is ignored in this case.
(3) The ground voltage is given as zero at the cold side of the p-type element.

### 2.5. Numerical method and validation

The TEG model was built using ANSYS 12.0.1 software. The discretization of the governing equations and the finite element formulation were obtained using the Galerkin method [37]. When the simulation was finished, the results of the TEG performance, including the heat supplied to the hot side $Q_h$, the generated current $I$, the output power $P$, and the efficiency $\eta_{TE} = P/Q_h$, were obtained.

The validation of the proposed TEG model was performed, and the results were compared with those of Chen et al. [8]. The TE geometry was chosen to be consistent with Chen's; that is, the values of 1.6 mm, 1.4 mm, and 1.4 mm corresponding to the TE element length, width, and depth, respectively. The external load resistance $R_L$ was set to 0.0268 Ω. The assumptions of $S_p = -S_n$, $k_p = k_n$, and $\rho_{e,p} = \rho_{e,n}$, which are considered reasonable [25], were made to reduce the number of variables. The obtained material properties are listed in Table 1.

The simulation was conducted using the above geometry and material properties as well as the boundary conditions mentioned earlier. The case without heat loss was first examined. Orthogonal grids were used for the simulation. Three grid systems of 2,432, 4,600, and 12,544 grids were individually tested to check the grid independence. According to assumption (5), heat supplied to the hot side $Q_h$ and the output power $P$ of the TEG module can be calculated from the corresponding results of the TEG model by multiplying them by the number of thermoelectric couples. The numerical results and the analytical results are summarized in Table 2. Good agreement can be found between the numerical and analytical results. In addition, the obtained physical values in terms of the three grid systems used are equivalent, as shown in Table 2. Therefore, the second grid system (4600) is adopted for simulations.

The case with heat loss was examined next; the results are shown in Fig. 2. In the figure, $Q_h$ and $\eta_{TE}$ obtained in the present study for various heat transfer coefficients $h_{loss}$ are compared with those reported by Chen et al. [8]. The trends of $Q_h$ and $\eta_{TE}$ are close to those of Chen's. The maximum relative errors between the numerical results and the literature data are less than 10%, revealing that validity of the present prediction. The slight deviation may be caused by the difference between the derived and actual material properties, which are temperature-dependent.

**Table 3**
Properties of heat sink system [40].

| Material | Property |
|---|---|
| Aluminum (for fin) | $k_f = 237$ W/m K |
| Air (for coolant) | $k_g = 26.3 \times 10^{-3}$ W/m K |
| | $\rho = 1.1614$ kg/m$^3$ |
| | $\mu = 184.6 \times 10^{-7}$ N s/m$^2$ |
| | $\alpha = 22.5 \times 10^{-6}$ m$^2$/s |
| | $C_p = 1007$ J/kg K |
| | $\nu = 15.89 \times 10^{-6}$ m$^2$/s |

## 3. Results and discussion

### 3.1. Influence of heat sink geometry (the first-stage optimization)

In order to investigate the influence of heat sink geometry, the heat sink configuration from Loh et al. [38] is selected. Because their heat sink was used to cool a thermoelectric module, it is suitable for

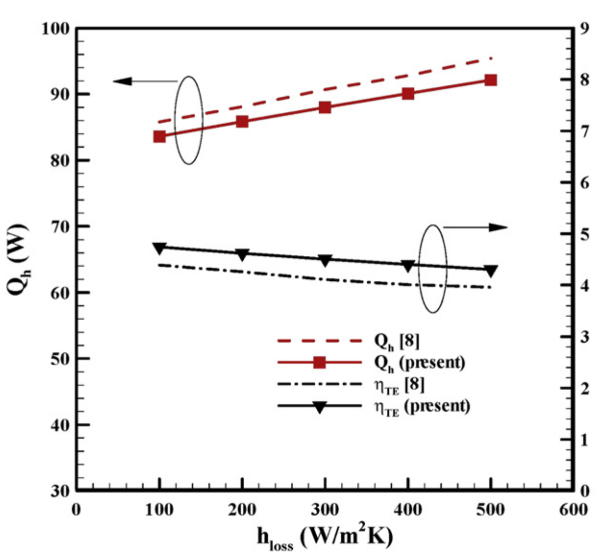


**Fig. 2.** Comparisons of TEG performance between the numerical results and literature data ($T_h = 423$ K and $T_c = 303$ K).

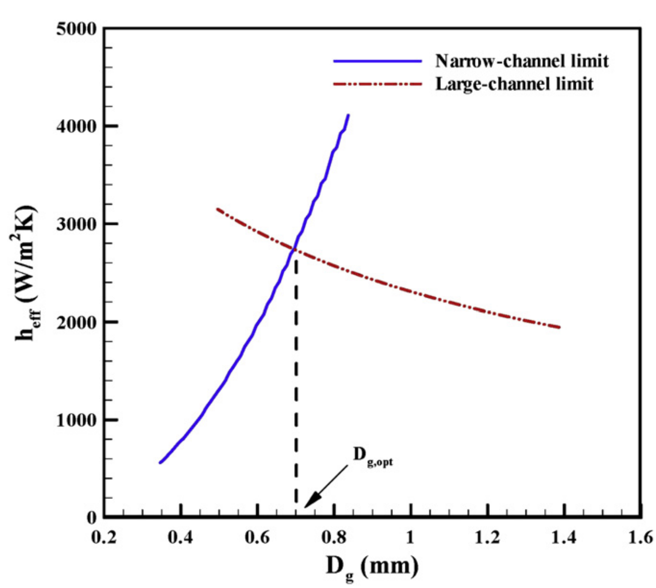


**Fig. 3.** Development of the effective heat transfer coefficient for various values of $D_g$.

this study. The base case of the geometry had heat sink length $L_{HS} = 20$ mm, heat sink width $W_{HS} = 40$ mm, fin height $H_f = 14$ mm, and fin thickness $t_f = 0.2$ mm. In addition, the pressure drop across the heat sink was fixed at 40 Pa [39]. The material properties applied to the heat sink are listed in Table 3 [40]. The TEG geometry was 1 mm ($W_{TE}$) × 1 mm ($D_{TE}$) × 1 mm ($L_{TE}$). Consequently, the development of the effective heat transfer coefficient of the heat sink for various fin spacings can be obtained from the analytical method mentioned earlier; the results are shown in Fig. 3. In the figure, the two curves corresponding to the two extreme limits intersect at a point which identifies the optimal fin spacing $D_{g,opt}$ and the corresponding effective heat transfer coefficient. Further comparisons of the TEG performance, namely the output power and efficiency, can be found in Fig. 4a and b, respectively, where the cases for $0.5D_{g,opt}$, $D_{g,opt}$, and $2D_{g,opt}$ are shown. The effective heat transfer coefficient of $0.5D_{g,opt}$ and $2D_{g,opt}$ can be derived from Eq. (8) and Eq. (9), respectively. As shown in Fig. 4, there is a maximum value in each curve (the electrical current was varied by altering the external loading). In addition, the case of $D_{g,opt}$ covers the widest range of the generated current and offers the maximum output power and efficiency, as illustrated in Fig. 4a and b, respectively. Therefore, the results elucidate the importance of the heat sink optimization on TEG performance, as reported by Astrain et al. [16]. It is noteworthy that the optimal values of the current corresponding to the maximum output power and the maximum efficiency do not coincide.

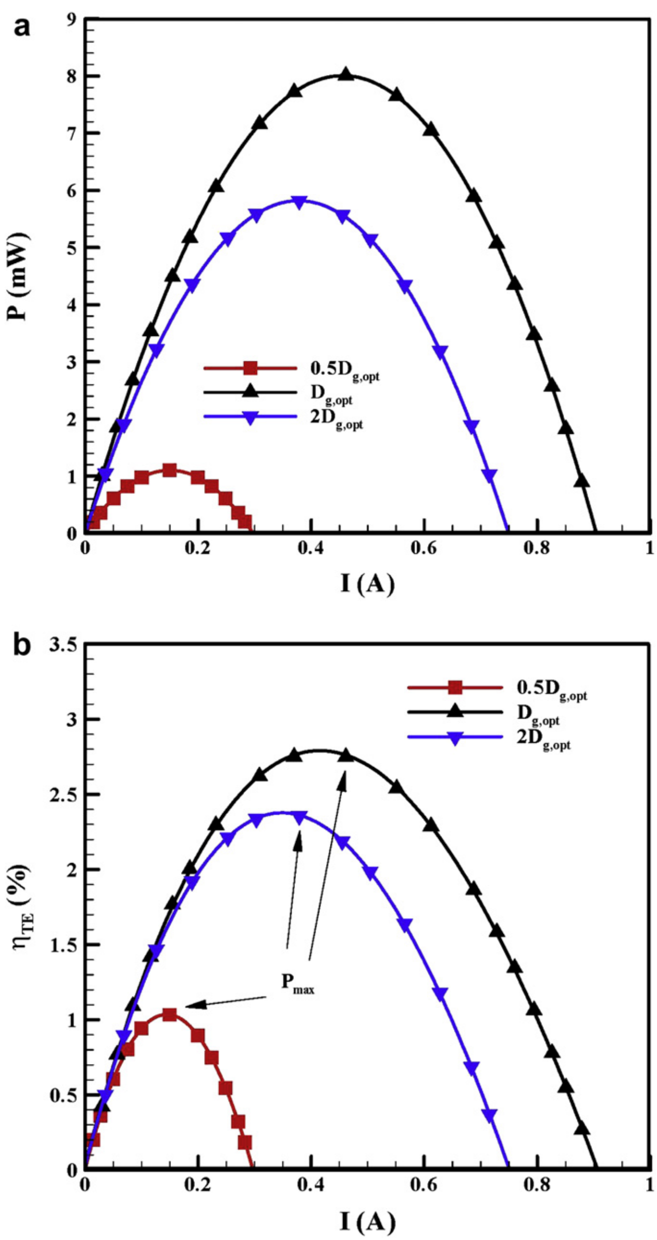


**Fig. 4.** Effect of fin spacing on (a) TEG output power and (b) TEG efficiency.

In order to investigate the influence of external loading, the output powers at various resistance ratios of external loading to the TEG couple are shown in Fig. 5. Instead of a parabolic curve, the curves are more like Gaussian distributions in a log–log plot. The optimal resistance ratios corresponding to the maximum output power deviate from one slightly; that is, if the thermal resistance of the heat sink is considered at the cold side of the TEG couple, an optimal external resistance larger than the TEG internal resistance is needed to achieve the maximum output power. The optimal external resistance is equal to the TEG internal resistance only when the thermal resistance of the heat sink reduces to zero. For simplicity, only the maximum power or power density is considered in the following discussion.

After the optimal fin spacing of the heat sink was found, the other geometry parameters were varied. The procedure was as follows: (1) set the heat sink geometry; (2) determine the optimal fin spacing; (3) calculate the effective heat transfer coefficient of the heat sink; and (4) evaluate the performance of the TEG and the heat sink. In the following section, the output power density is discussed. Moreover, the heat sink efficiency is considered as the heat sink performance; it can be determined as [40]:

$$\eta_{HS} = 1 - \frac{N_f A_f}{A_t}\left(1 - \eta_f\right) \tag{12}$$

where $N_f$ is the number of fins, $A_f$ is the surface area of each fin, $A_t$ is the total heat sink heat transfer area, and $\eta_f$ is the fin efficiency, which can be obtained as:

$$\eta_f = \frac{\tan h\left(mH_f\right)}{mH_f} \tag{13}$$

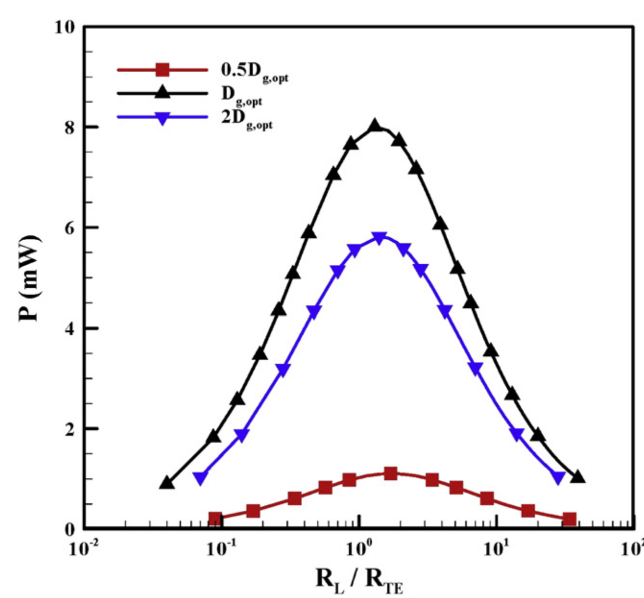


**Fig. 5.** Effect of external loading on TEG output power.

**Table 4**
Dimensions of heat sink for each case.

| Parameters | $V$ (mm$^3$) | $L_{HS}$ (mm) | $W_{HS}$ (mm) | $H_f$ (mm) | $t_f$ (mm) |
|---|---|---|---|---|---|
| Base case | 11,200 | 20 | 40 | 14 | 0.2 |
| Case 1-1 | | 10, 15, 20, 30, 40 | $40\sqrt{2}$, $40\sqrt{4/3}$, 40, $40/\sqrt{2/3}$, $40/\sqrt{2}$ | $14\sqrt{2}$, $14\sqrt{4/3}$, 14, $14/\sqrt{2/3}$, $14/\sqrt{2}$ | |
| 1-2 | | | 80, 160/3, 40, 80/3, 20 | 14 | |
| 1-3 | | | 40 | 28, 56/3, 14, 28/3, 7 | |
| Case 2 | | 20 | 20, 30, 40, 60, 80 | 28, 56/3, 14, 28/3, 7 | |
| Case 3 | | 20 | 40 | 14 | 0.1, 0.15, 0.2, 0.3, 0.4 |

where $m$ is defined as:

$$m = \sqrt{\frac{\bar{h}P_f}{k_f A_{c,f}}} \tag{14}$$

In the preceding equation, $P_f$ represents the fin perimeter, $A_{c,f}$ is the fin cross-sectional area, $k_f$ is the fin thermal conductivity, and $\bar{h}$ is the average heat transfer coefficient obtained from the analytical model proposed by Teertstra et al. [34].

It is worth noting that the overall heat sink volume ($V = W_{HS} \times L_{HS} \times H_f$) is fixed and the geometry parameter $X$ (i.e., $L_{HS}$, $W_{HS}$, $H_f$, and $t_f$) is considered in the range of $0.5X_{base} \leq X \leq 2X_{base}$, where $X_{base}$ is the geometry parameter of the base case. In this study, three cases are considered: varying $L_{HS}$ (Case 1), determining $W_{HS}$ by varying $H_f$ with a fixed $L_{HS}$ (Case 2), and varying $t_f$ (Case 3). Because the overall heat sink volume is fixed, Case 1 can be further separated into three sub-cases, namely, determining $L_{HS}$ by varying $W_{HS}H_f$ (Case 1-1), determining $L_{HS}$ by varying $W_{HS}$ (Case 1-2), and determining $L_{HS}$ by varying $H_f$ (Case 1-3). The detailed dimensions of the heat sink for each case are summarized in Table 4. The TEG and heat sink performance results for each case are shown in Figs. 6–8, respectively. Copeland [41] showed that shorter heat sinks had better performance in terms of thermal conductance. Fig. 6 shows that the three sub-cases of Case 1 enhance the TEG output power density but decrease the heat sink efficiency when $L_{HS}$ is decreased. Similar trends can be seen in Figs. 7 and 8. In addition, the TEG performance range is large for Case 1, whereas that for Case 3 is small. The results imply that the effect of the fin thickness on TEG performance is relatively slight. Although Case 1 can offer larger TEG power density, the drop in heat sink efficiency is significant. It is thus difficult to evaluate the best choice when the TEG and heat sink performance are considered simultaneously. Therefore, an alternative approach named compromise programming is carried out in the following section.

### 3.2. Compromise programming (second-stage of optimization)

To determine a compromise between the TEG power density and heat sink efficiency, a multi-objective optimization method called compromise programming is utilized. This method is

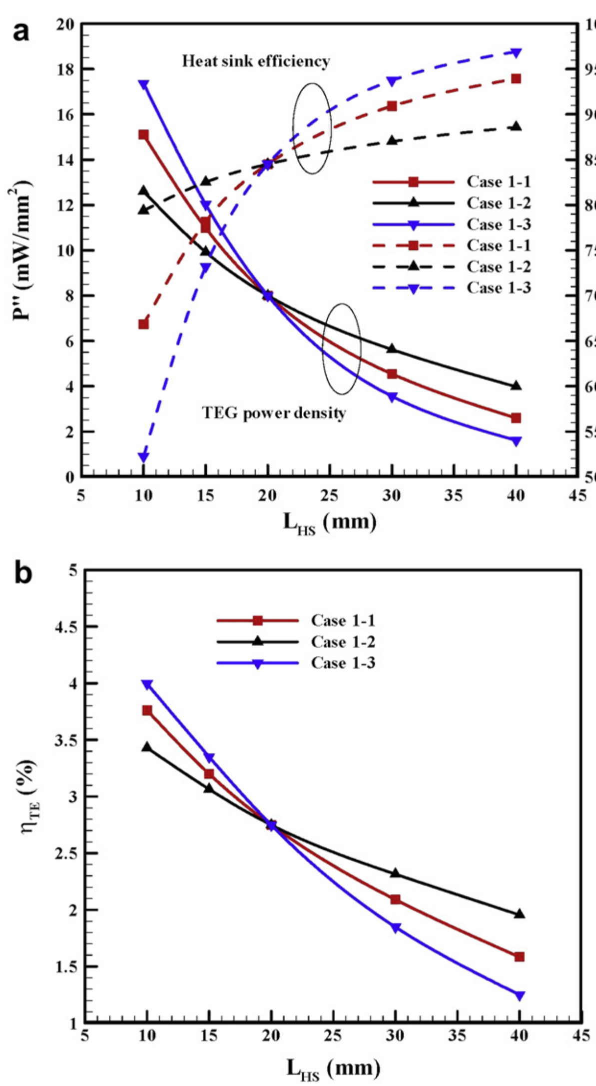


**Fig. 6.** Numerical results for Case 1. (a) TEG power density and heat sink efficiency and (b) TEG efficiency.

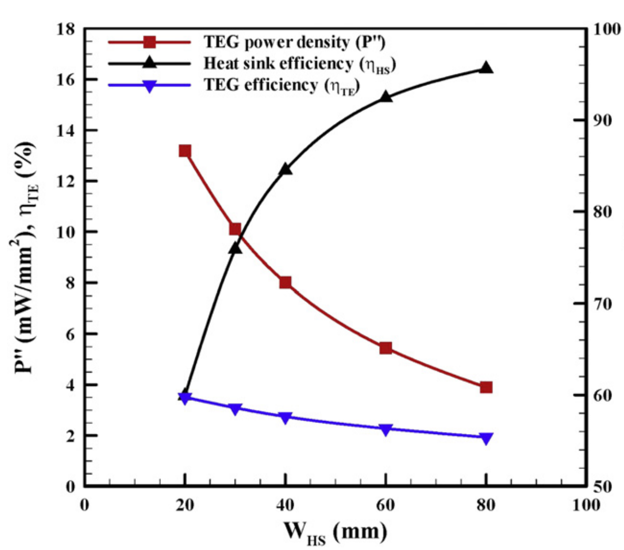


**Fig. 7.** TEG and heat sink performances for Case 2.

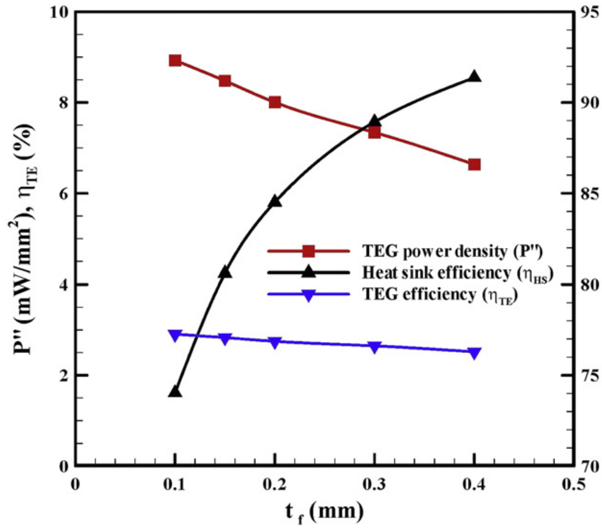


**Fig. 8.** TEG and heat sink performances for Case 3.

a well-known approach in operation research and management science [42]. The following simple form is applied in this study:

$$f = \left( \left( \frac{x - x^*}{x^*} \right)^2 + \left( \frac{y - y^*}{y^*} \right)^2 \right)^{1/2} \tag{15}$$

where $(x,y)$ represents the real point, $(x^*,y^*)$ is the ideal point, and $f$ is the distance function. In practical applications, the heat sink efficiency and the TEG power density are considered as $x$ and $y$, respectively. For example, the compromise programming operation for Case 1 is shown in Fig. 9. If a heat sink efficiency of 100% and the TEG power density at the conditions of $T_h = 423$ K and $T_c = 303$ K (25.59 mW mm$^{-2}$) are regarded as the ideal point $(x^*,y^*)$, the distance to each real point can be determined using Eq. (15). The point that has the minimum distance for Case 1-1, called the compromise point, is shown in Fig. 10. In this case, though the heat sink efficiency is reduced by a factor of 20.93%, the power density

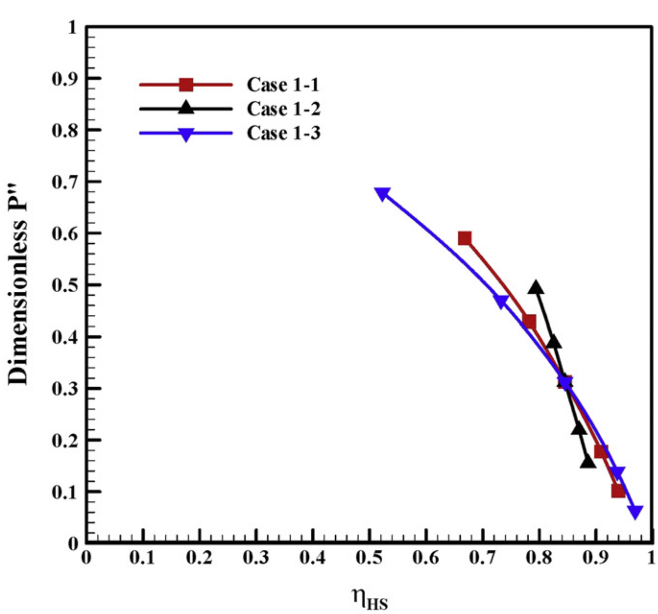


**Fig. 9.** Curves obtained using compromise programming.

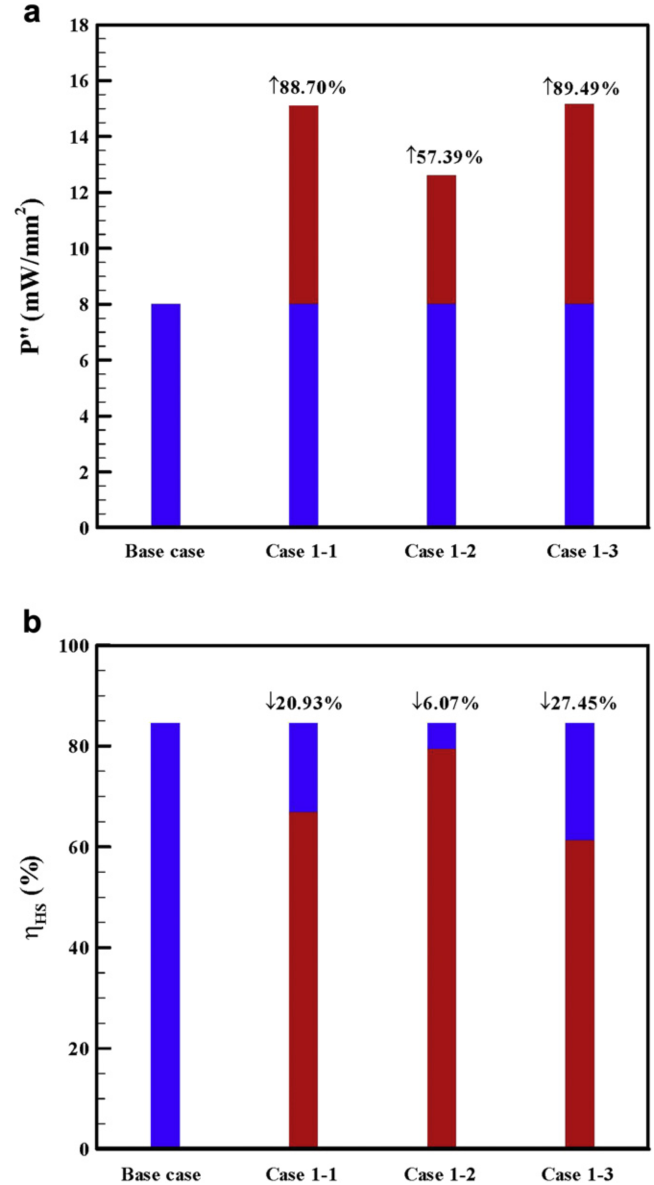


**Fig. 10.** TEG performance at compromise points for the sub-cases of Case 1 obtained using the compromise programming. (a) TEG power density and (b) heat sink efficiency.

can be enhanced by 88.70% compared to those of the base case. If this case is compared with the results of the other geometry parameters, say, Case 2 and Case 3, the results shown in Fig. 11 indicate that Case 1-1, where $L_{HS}$ is reduced by increasing $W_{HS}H_f$, is the best choice when the TEG and heat sink performance are considered simultaneously. Moreover, as mentioned earlier, the effect of $t_f$ on the TEG and heat sink performances is negligible even when the best compromise point is obtained.

### *3.3. Scaling effect on TEG performance*

As mentioned above, the case of determining $L_{HS}$ by varying $W_{HS}H_f$ is the recommended approach for achieving the best compromise between the TEG and heat sink performances. Therefore, the scaling effect on the TEG performance is taken into account in this case for further investigation. In order to keep the thermal conductance and electric resistance of the TE couples

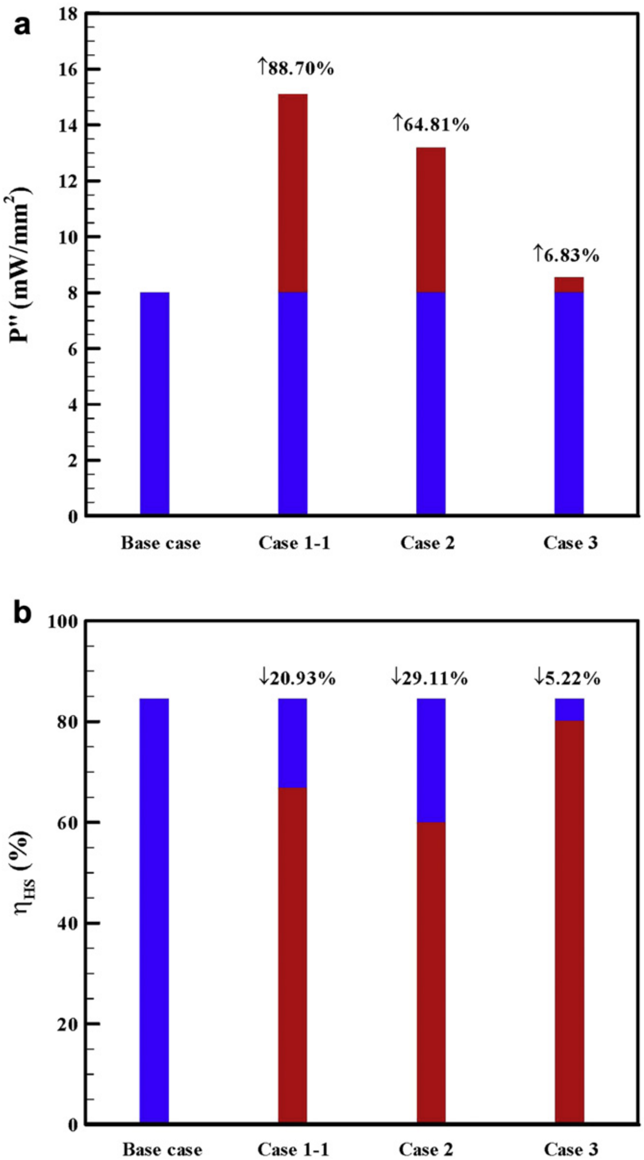


**Fig. 11.** TEG performance at compromise points for three cases obtained using compromise programming. (a) TEG power density and (b) heat sink efficiency.

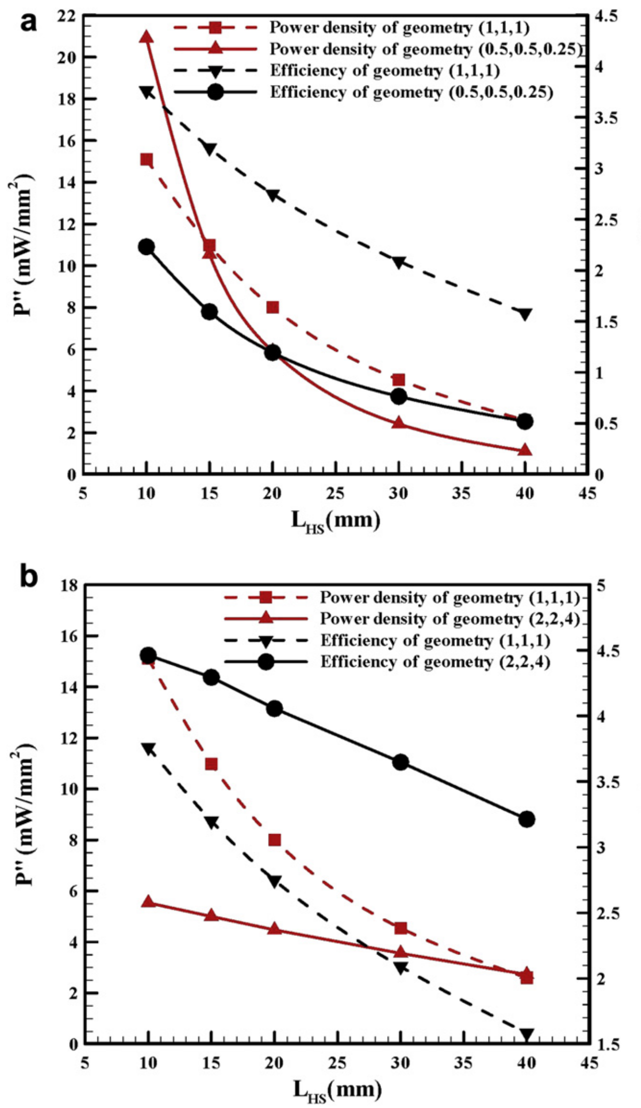


**Fig. 12.** (a) Scaling-down effect on TEG performance and (b) scaling-up effect on TEG performance.

constant, the scaling approach with a constant geometry factor ($A_{c,\mathrm{TE}}/L_{\mathrm{TE}}$) is employed [2]. Accordingly, three kinds of the TEG geometry ($W_{\mathrm{TE}}$, $D_{\mathrm{TE}}$, $L_{\mathrm{TE}}$) with the same geometry factor are considered: the base case (1 mm, 1 mm, 1 mm), the scaling-down case (0.5 mm, 0.5 mm, 0.25 mm), and the scaling-up case (2 mm, 2 mm, 4 mm). The scaling-down effect on TEG performance is shown in Fig. 12a and the scaling-up effect on TEG performance is shown in Fig. 12b. In Fig. 12a, a larger output power density can be obtained by scaling-down the TEG size when the heat sink length $L_{\mathrm{HS}}$ is below about 14.5 mm. This implies that the drop in cross-section area of the TEG is smaller than that in output power and thus a larger power density is obtained when $L_{\mathrm{HS}}$ is below 14.5 mm. Therefore, the heat sink design is a key point for the scaling-down case. However, the power density cannot be improved by scaling-up the TEG size under the considered range of $L_{\mathrm{HS}}$ as shown in Fig. 12b. The lower power density is due to the fact that the increase in output power is lower than that in cross-section area of the TEG for the scaling-up case. The efficiency of the larger TEG is better due to the larger temperature difference across the TEG elements.

## 4. Conclusions

A TEG combined with an air-cooling system has been investigated in this study through a method of two-stage optimization for designing heat sink geometry. An analytical method is employed to model the air-cooling system and the finite element method is utilized to simulate performance of the TEG. In the first-stage optimization, an analytical method using the concept of effective heat transfer coefficient is adopted to design the optimal fin-to-fin spacing of the heat sink. The results show that better TEG performance can be achieved after the first-stage of optimization. The optimal resistance ratio of external loading to the TEG couple slightly deviates from one. In the second-stage optimization, the compromise programming method, a compromise between the TEG performance and the heat sink performance is obtained when the heat sink volume is fixed. The results suggest that decreasing the length of heat sink by increasing the frontal area ($W_{\mathrm{HS}}H_f$) of the heat sink is the best approach. In this case, at the compromise point, the TEG output power density is improved by 88.70% and the heat sink efficiency is reduced by only 20.93% compared to the base case. The influence of the fin thickness is negligible even when the best

compromise point is found. The power density of the TEG can be further enhanced by scaling-down the TEG size with a constant geometry factor when the heat sink length is below 14.5 mm. Alternatively, the power density cannot be improved by scaling-up the TEG size. However, a better efficiency is obtained by scaling-up the TEG size due to a larger temperature difference across the TEG. The results have provided a useful guideline for designing TEGs combined with an air-cooling system.

## Acknowledgments

The authors acknowledge the financial support by the National Science Council, Taiwan, ROC, on this research.

## References

[1] Simons RE, Ellsworth MJ, Chu RC. An assessment of module cooling enhancement with thermoelectric coolers. J Heat Transfer-Trans ASME 2005; 127:76–84.
[2] Wu KH, Hung CI. Thickness scaling characterization of thermoelectric module for small-scale electronic cooling. J Chin Soc Mech Eng 2009;30:475–81.
[3] Cheng TC, Cheng CH, Huang ZZ, Liao GC. Development of an energy-saving module via combination of solar cells and thermoelectric coolers for green building applications. Energy 2011;36:133–40.
[4] Chen WH, Liao CY, Hung CI. A numerical study on the performance of miniature thermoelectric cooler affected by Thomson effect. Appl Energy 2012;89: 464–73.
[5] Champier D, Bedecarrats JP, Rivaletto M, Strub F. Thermoelectric power generation from biomass cook stoves. Energy 2010;35:935–42.
[6] Champier D, Bedecarrats JP, Kousksou T, Rivaletto M, Strub F, Pignolet P. Study of a TE (thermoelectric) generator incorporated in a multifunction wood stove. Energy 2011;36:1518–26.
[7] Martinez A, Astrain D, Rodriguez A. Experimental and analytical study on thermoelectric self cooling of devices. Energy 2011;36:5250–60.
[8] Chen M, Rosendahl LA, Condra T. A three-dimensional numerical model of thermoelectric generators in fluid power systems. Int J Heat Mass Transfer 2011;54:345–55.
[9] Disalvo FJ. Thermoelectric cooling and power generation. Science 1999;285: 703–6.
[10] Cheng CH, Huang SY, Cheng TC. A three-dimensional theoretical model for predicting transient thermal behavior of thermoelectric coolers. Int J Heat Mass Transfer 2010;53:2001–11.
[11] Hsu CT, Huang GY, Chu HS, Yu B, Yao DJ. Experiments and simulations on low-temperature waste heat harvesting system by thermoelectric power generators. Appl Energy 2011;88:1291–7.
[12] Chen G. Nanoscale energy transport and conversion. Oxford: Oxford University Press; 2005.
[13] Bell LE. Cooling, heating, generating power, and recovering waste heat with thermoelectric systems. Science 2008;321:1457–61.
[14] Esarte J, Min G, Rowe DM. Modelling heat exchangers for thermoelectric generators. J Power Sources 2001;93:72–6.
[15] Chen L, Gong J, Sun F, Wu C. Effect of heat transfer on the performance of thermoelectric generators. Int J Therm Sci 2002;41:95–9.
[16] Astrain D, Vian JG, Martinez A, Rodriguez A. Study of the influence of heat exchangers' thermal resistances on a thermoelectric generation system. Energy 2010;35:602–10.
[17] Noie-Baghban SH, Majideian GR. Waste heat recovery using heat pipe heat exchanger (HPHE) for surgery rooms in hospitals. Appl Therm Eng 2000;20: 1271–82.
[18] Chen WH. Waste burning and heat recovery characteristics of a mass burn incineration system. J Air Waste Manage Assoc 2003;53:136–42.
[19] Chen WH, Chung YC, Liu JL. Analysis on energy consumption and performance of reheating furnaces in a hot strip mill. Int Commun Heat Mass Transfer 2005;32:695–706.
[20] Shih HY, Huang YC. Thermal design and model analysis of the Swiss-roll recuperator for an innovative micro gas turbine. Appl Therm Eng 2009;29: 1493–9.
[21] Chen WH, Chiu TW, Hung CI. Enhancement effect of heat recovery on hydrogen production from catalytic partial oxidation of methane. Int J Hydrogen Energy 2010;35:7427–40.
[22] Chen WH, Syu YJ. Thermal behavior and hydrogen production of methanol steam reforming and autothermal reforming with spiral preheating. Int J Hydrogen Energy 2011;36:3397–408.
[23] Hsiao YY, Chang WC, Chen SL. A mathematic model of thermoelectric module with applications on waste heat recovery from automobile engine. Energy 2010;35:1447–54.
[24] Gou X, Xiao H, Yang S. Modeling, experimental study and optimization on low-temperature waste heat thermoelectric generator system. Appl Energy 2010;87:3131–6.
[25] Meng F, Chen L, Sun F. A numerical model and comparative investigation of a thermoelectric generator with multi-irreversibilities. Energy 2011;36: 3513–22.
[26] Xuan XC. Optimum design of a thermoelectric device. Semicond Sci Technol 2002;17:114–9.
[27] Kubo M, Shinoda M, Furuhata T, Kitagawa K. Optimization of the incision size and cold-end temperature of a thermoelectric device. Energy 2005;30: 2156–70.
[28] Yilbas BS, Sahin AZ. Thermoelectric device and optimum external load parameter and slenderness ratio. Energy 2010;35:5380–4.
[29] Jang B, Han S, Kim JY. Optimal design for micro-thermoelectric generators using finite element analysis. Microelectron Eng 2011;88:775–8.
[30] Yang YT, Peng HS. Numerical study of pin-fin heat sink with un-uniform fin height design. Int J Heat Mass Transfer 2008;51:4788–96.
[31] Sharp J, Bierschenk J, Lyon Jr HB. Overview of solid-state thermoelectric refrigerators and possible applications to on-chip thermal management. Proc IEEE 2006;94:1602–12.
[32] Duan Z, Muzychka YS. Experimental investigation of heat transfer in impingement air cooled plate fin heat sinks. J Electron Packag 2006;128: 412–8.
[33] Antonova EE, Looman CC. Finite elements for thermoelectric device analysis in ANSYS. 24th International Conference on Thermoelectrics 2005: 215–218.
[34] Teertstra P, Yovanovioch MM, Culham JR. Analytical forced convection modeling of plate fin heat sinks. 15th IEEE SEMI-THERM Symposium 1999: 34–41.
[35] Mereu S, Sciubba E, Bejan A. The optimal cooling of a stack of heat generating boards with fixed pressure drop, flowrate or pumping power. Int J Heat Mass Transfer 1993;36:3677–86.
[36] Bello-Ochende T, Liebenberg L, Meyer JP. Constructal cooling channels for micro-channel heat sinks. Int J Heat Mass Transfer 2007;50:4141–50.
[37] Silvester PP, Ferrari RL. Finite elements for electrical engineers. 3rd ed. New York: Cambridge University Press; 1996.
[38] Loh CK, Nelson D, Chou DJ. Thermal characterization of fan-heat sink systems in miniature axial fan and micro blower airflow. Proc of the 17th IEEE Semi-Therm Symposium 2001: 111–116.
[39] Copeland D. Optimization of parallel plate heatsinks for forced convection. Proc of the 16th IEEE Semi-Therm Symposium 2000:266–272.
[40] Incropera FP, Dewitt DP, Bergman TL, Lavine AS. Fundamentals of heat and mass transfer. 6th ed. Hoboken: John Wiley & Sons; 2007.
[41] Copeland DW. Fundamental performance limits of heatsinks. J Electron Packag 2003;125:221–5.
[42] Moron MA, Romero C, Ruiz Del Portal FR. Generating well-behaved utility functions for compromise programming. J Optim Theory Appl 1996;91: 643–9.